PHYSICAL REVIEW B **72**, 064401 (2005)

Magnetic and transport properties of the layered perovskite system $Sr_{2-y}Y_yCoO_4$ $(0 \leqslant y \leqslant 1)$

X. L. Wang[1,2] and E. Takayama-Muromachi[1,*]

[1]*Superconducting Materials Center, National Institute for Materials Science, 1-1 Namiki, Tsukuba, Ibaraki 305-0044, Japan*

[2]*Spintronic and Electronic Materials Group, Institute for Superconducting and Electronic Materials, University of Wollongong, Northfield Ave. NSW 2522, Australia.*

(Received 20 May 2004; revised manuscript received 18 January 2005; published 1 August 2005)

Layered perovskite cobalt oxides $Sr_{2-y}Y_yCoO_4$ ($y=0$, 0.1, 0.3, 0.5, 0.67, 0.83, and 1) were synthesized under high pressure and high temperature conditions. Structure refinement revealed that these compounds crystallize in K_2NiF_4-type structures with space group I4/mmm. The parent compound Sr_2CoO_4 undergoes a ferromagnetic transition with $T_c=255$ K. The T_c decreases with increasing y to 150 K for $y=0.5$, and ferromagnetism was not observed for $y \geqslant 0.67$. Assessment of spin states for Co^{3+} and Co^{4+} ions suggested strongly that both are present as intermediate spin states when $y \leqslant 0.67$ at least for the higher temperature range above T_c. Fairly large negative magnetoresistance was observed for Sr_2CoO_4 in the vicinity of T_c and in the lower temperature region.

DOI: 10.1103/PhysRevB.72.064401 PACS number(s): 75.30.Cr, 72.80.Ga, 75.47.−m

I. INTRODUCTION

Cobalt oxide perovskite $LaCoO_3$ and its divalent substitutions have intrigued many researchers because of their complex electronic and magnetic properties (see Ref. 1). Their rich physical properties are related to the closeness of the crystal field splitting Δ_{cf} and the exchange energy (Hund's rule coupling) Δ_{ex} of Co^{3+} in the octahedral coordination, with a small energy difference between the low-spin (LS) state ($t_{2g}^6, S=0$) and the high-spin (HS) state ($t_{2g}^4e_g^2, S=2$) or the intermediate-spin (IS) state ($t_{2g}^5e_g^1, S=1$). At low temperatures, $LaCoO_3$ is a nonmagnetic insulator with the LS state of Co^{3+}. Upon heating, its magnetic susceptibility increases and has a broad maximum at ~90 K, then shows a Curie-Weiss type decrease. Some theoretical[2,3] and experimental[4–7] studies have proposed that this behavior is caused by a spin state transformation from LS to IS, but the appearance of the IS state is still controversial and remains to be studied.

The Sr doped system of $La_{1-x}Sr_xCoO_3$ has also been extensively studied and it is well known that the hole doping affects the spin state of Co^{3+} in a similar way to temperature (see Ref. 8). Upon the Sr doping, the system changes from nonmagnetic insulator to ferromagnetic metal. For the $x=0.5$ phase, Goodenough proposed an intermediate-spin model with t_{2g}^5 localized electrons and σ^* itinerant electrons at a density of 0.5 per Co atom.[9] Later, his group proposed a revised model and a detailed temperature-composition (x) phase diagram of the system.[8] The hole doped system may become further complicated because Co^{4+} ions can also exist in several spin-state configurations like Co^{3+}.[10–12]

It is well known that the dimensionality of a system is a key factor governing its electronic structure, and thus, two-dimensional (2D) layered cobalt oxides are quite interesting to compare with the three-dimensional (3D) perovskites. Thus far, various studies have been carried out on K_2NiF_4-type cobalt oxides,[13–20] although the number of reports is relatively small compared with the 3D perovskite system. A K_2NiF_4-type oxide consists of CoO_2 planes separated by rock-salt-type planes, and its 2D nature reduces the bandwidth of e_g electrons as compared to the 3D network. This seems a key difference between the two systems. Moritomo *et al.* investigated the K_2NiF_4-type system of $La_{2-x}Sr_xCoO_4$ with a mixed valence of Co^{2+} and Co^{3+} and found steep decreases in the effective magnetic moment, Weiss temperature, and electrical resistivity with x increasing beyond ~0.7.[16] In accordance with these results, they proposed a spin state transition of the Co^{3+} ion from HS to IS. However, Wang *et al.* have reported that the IS state never becomes the ground state of $LaSrCoO_4$ according to their theoretical studies using the unrestricted Hartree-Fock approximation and the real-space recursion method.[19,20]

In the present study, we have developed a K_2NiF_4-type cobalt oxide with only Co^{4+} ions, Sr_2CoO_4, using a high pressure and high temperature technique. This compound exhibits a ferromagnetic transition with $T_c=255$ K. The spin state of Co^{4+} appears to be the IS state, at least in the higher temperature range above T_c. Negative magnetoresistance has been observed at both low temperatures and in the vicinity of T_c. Moreover, we carried out partial substitution of Y for Sr, i.e., electron doping, and studied the substitution effects on the structural, magnetic, and transport properties, and the spin states for the $Sr_{2-y}Y_yCoO_4$ system. Assessment of the spin state for the Co^{3+} (produced by introduction of Y^{3+} for Sr^{2+}) and Co^{4+} ions suggested strongly that both are present as IS states at least in the higher temperature range.

II. EXPERIMENT

Polycrystalline samples of $Sr_{2-y}Y_yCoO_4$ ($y=0$, 0.1, 0.3, 0.5, 0.67, 0.83, and 1) were prepared as follows. Fine and pure powders of SrO_2, Co, and Y_2O_3 were well mixed in the atomic ratio Sr:Y:Co$=2-y:y:1$. Approximately 0.2 g of each mixture was placed in a gold capsule and then compressed at 6 GPa in a high pressure apparatus which was originally developed in our institute. The samples were

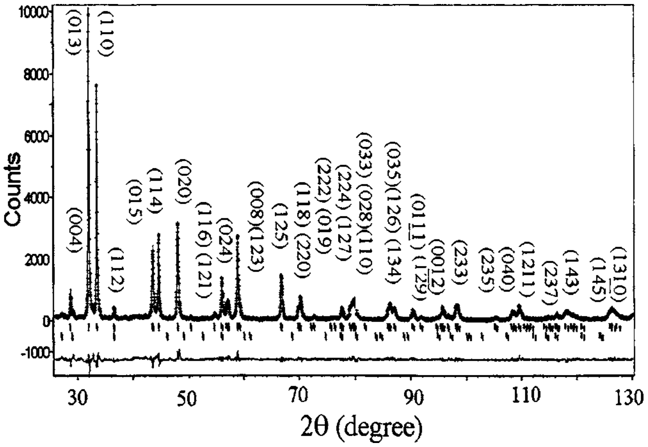

FIG. 1. The observed (crosses), calculated (solid line), and difference diffraction (bottom solid line) profiles at 300 K for Sr_2CoO_4. The top peak markers relate to Sr_2CoO_4 while the lower peak markers pertain to the impurity SrO_2. All the indexed peaks belong to the Sr_2CoO_4 phase.

then heated at 1000 °C–1350 °C for 1–3 hours and quenched to room temperature followed by release of pressure. The high-pressure phases in the samples were identified using powder x-ray diffraction. Structure refinements were carried out by the Rietveld method using the RIETICA program.[21] Magnetic and magnetotransport properties were investigated using commercial Quantum Design MPMS and PPMS systems between 2 and 330 K in magnetic fields up to 7 T.

III. RESULTS AND DISCUSSION

Figure 1 shows the results of Rietveld refinement of the XRD pattern of Sr_2CoO_4 measured at room temperature. The pattern could be indexed when based on a tetragonal unit cell similar to that of Sr_2TiO_4.[22] Close examination of the diffraction profile revealed the presence of a small amount of SrO_2 in this sample, which was included in the refinement as a second phase. The initial structural model for the refinement was taken from that of Sr_2TiO_4.[23] The refined structure of Sr_2CoO_4 was found to be of the K_2NiF_4 type with space group I4/mmm. A schematic representation of the structure of Sr_2CoO_4 is shown in Fig. 2. The weight percentage of the impurity phase of SrO_2 in the sample was refined to be 1.2 (1) %. As can be seen from Fig. 1, the calculated pattern is in excellent agreement with the observed one. The atomic parameters, isotropic temperature factors, and Co-O bond lengths are summarized in Table I.

The structure of Sr_2CoO_4 consists of corner-sharing CoO_6 octahedra with 2D CoO_2 planes separated by insulating double layers of SrO as shown in Fig. 2. The observed Co-O(1) and Co-O(2) bond lengths of 1.898 Å and 1.994 Å indicate that the octahedron is tetragonally distorted with elongation along the c axis. The Co-O(1) bond length is slightly smaller compared to that of 3D cubic $SrCoO_3$ (a=1.912 Å) which was made under high pressure.

Next, we carried out substitution of Y for Sr under the same high pressure conditions. The $Sr_{2-y}Y_yCoO_4$ samples were found to be almost single phase but with a trace amount of Y_2O_3 in a few cases. The XRD patterns of the samples can be indexed based on the K_2NiF_4 type unit cells whose dimensions are shown in Fig. 3 as a function of y. It can be seen that both a and c decrease gradually with increasing y, except for the $y=1$ sample whose a-dimension is slightly larger than that of the $y=0.83$ sample. The decrease in the lattice parameters is in agreement with the fact that the size of the Y^{3+} ion is smaller than that of Sr^{2+}. The XRD patterns for $Sr_{1.5}Y_{0.5}CoO_4$ and $SrYCoO_4$ ($y=0.5,1$) were analyzed by the Rietveld method, and the crystallographic data obtained are shown in Table I where they are compared with those for Sr_2CoO_4. Refinement results indicated that for $y=0.5$, the in-plane Co-O(1) bond length (1.876 Å) is slightly shorter compared to that for $y=0$ (1.898 Å), while the Co-O(2) bond distance along the c axis is longer (2.030 Å) compared to $y=0$ (1.994 Å). This indicated that the Y^{3+} doping caused, at least up to $y=0.5$, a contraction of the Co-O bonds within the ab plane together with elongation along the c axis, yielding more distortion of the CoO_6 octahedron compared with the undoped Sr_2CoO_4. However, further doping to $y=1.0$ makes the Co-O(2) bond length smaller so that it has nearly the same value as the Co-O(1) length as is shown in Fig. 4. An anomalous variation is also seen in the c/a ratio in Fig. 3 where the c/a ratio decreases steeply beyond $y\sim 0.5$ consistent with the CoO_6 octahedron becoming less stretched along the c axis at $y=1.0$. We propose that these variations in the Co-O bond lengths and the lattice parameters are related to a particular spin state transition of the Co ion.

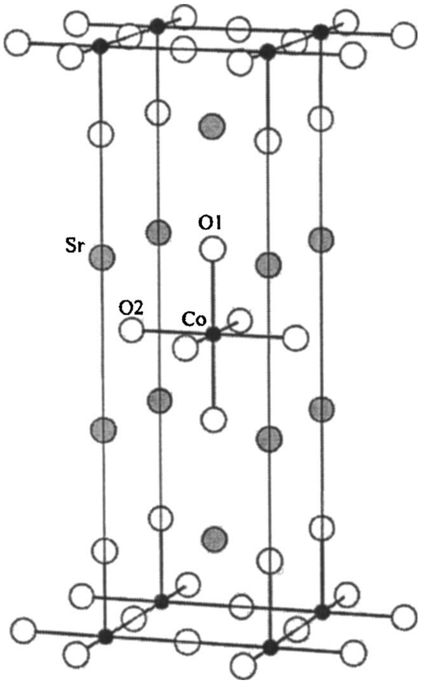

FIG. 2. Crystal structure of Sr_2CoO_4.

In Fig. 5, the temperature dependence of the electrical resistivity (ρ) is shown for the $Sr_{2-y}Y_yCoO_4$ system. Sr_2CoO_4 shows an almost temperature independent resistivity with a small negative coefficient. ρ at 300 K increases

TABLE I. Crystal data of $Sr_{2-y}Y_yCoO_4$ (y=0,0.5,1).

Atom	Wykoff site	x	y	z	B_{iso}[a]
Co	2e	0	0	0	0.41
					0.30
					0.30
Sr/Y	4e	0	0	0.3564	0.10
				0.3563	0.30
		0.3590	0.30		
O (1)	4c	0	0.5	0	1.15
					0.12
				0.46	
O (2)	4e	0	0	0.1592	1.29
				0.1646	1.11
				0.1628	0.83

Space group: I4/mmm

Lattice parameters (Å)			Bond length (Å):
a=3.7964(2)	c=12.4871(2)	Co-O(1):1.898	Co-O(2):1.994
3.7524(2)	12.3378(1)	1.876	2.030
3.7417(2)	12.0427(1)	1.871	1.910

Refinement factors R_p, R_B (%)

8.32, 2.5

8.26, 2.3

9.65, 3.3

[a] B_{iso} is an isotropic thermal parameter. Data on the first, second, and last lines are for the y=0, 0.5, and 1.0 samples, respectively.

with y from $\sim 7\times10^{-2}$ Ω cm for y=0 to 2×10^{3} Ω cm for y=1. Incidentally, the y=0.1 sample in Fig. 5 breaks the trend of monotonic increase of resistivity with y. The reason behind this is not clear at the moment.

Semiconducting behaviors are seen in samples with large y values. The ρ-T curves do not obey the thermal activation law, $\rho\sim\exp(-E_a/k_BT)$ where E_a and k_B stand for the activation energy and Boltzman constant, respectively. However, high temperature resistivity data could be approximately expressed by the thermal activation law, and the activation energies calculated for the data of $T>250$ K are shown in Fig. 5 as a function of y. The activation energy has an almost constant value of 10–20 meV for $y<0.5$, then steeply increases near x=0.5 to reach ~130 meV for y=1.0. As will be stated below, this y value of 0.5 corresponds to the point where ferromagnetism disappears.

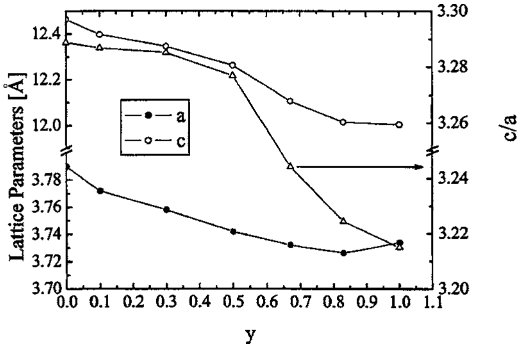

FIG. 3. Variations of lattice parameters of $Sr_{2-y}Y_yCoO_4$.

The temperature dependence of the field cooled dc magnetization measured at 20 Oe is shown in Fig. 6. Sr_2CoO_4 reveals a ferromagnetic transition with T_c=255 K, and T_c gradually decreases to 150 K for y=0.5. Ferromagnetism disappears for $y\geq0.67$. The field cooled magnetization was also measured at a high field of 2 kOe to obtain the inverse molar susceptibility, χ^{-1}, which is plotted against temperature in Fig. 7 for $y\leq0.67$. The χ^{-1} data above 250 K can be well fitted to the Curie-Weiss law; the Weiss temperature Θ and effective number of Bohr magnetons per Co ion $p_{eff}(\mu_B)$ are shown in Fig. 8. It can be seen that Θ decreases from 260 K for y=0 to −27.3 K for y=0.67, suggesting that the interaction between the magnetic moments

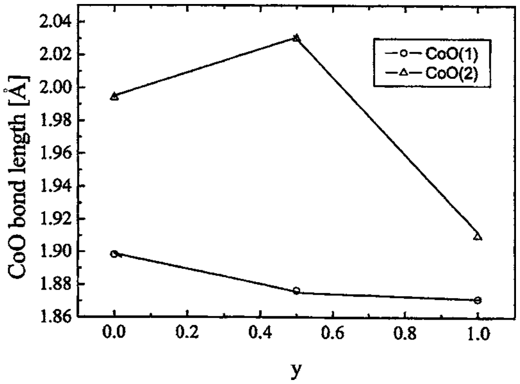

FIG. 4. Yttrium content (y) dependences of the Co—O(1) and Co—O(2) bond lengths.

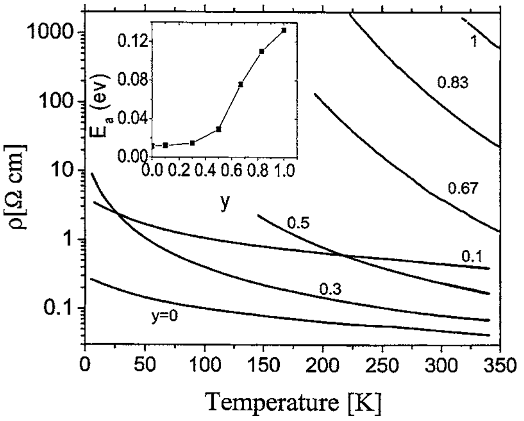

FIG. 5. Temperature dependence of the electrical resistivity (ρ) for the $Sr_{2-y}Y_yCoO_4$ system. Inset shows the activation energy, E_a.

changes from ferromagnetic to antiferromagnetic as y increases. p_{eff} is gradually reduced from 3.72 for $y=0$ to 3.01 for $y=0.67$.

As stated above, we observed semiconducting resistivities for the present system in the phases with large y values. Thus, a localized electron model may be a good starting point. In Fig. 9, the LS, IS, and HS states are schematically shown for the d^6 (Co^{3+}) and d^5 (Co^{4+}) configurations in a tetrahedral crystal field. This diagram based on the ionic model suggests that the spin state of Co^{4+} in Sr_2CoO_4 is the IS state because the value of p_{eff} observed (3.72) coincides with that expected for the spin only moment of the IS state Co^{4+} (3.87) whereas a very different value of 1.73 (5.92) is expected for the LS (HS) state. The p_{eff} decreases almost linearly with y, or rather with the Co^{3+} substitution for Co^{4+}, until $y=0.67$ (Fig. 8). This linear variation suggests that no spin state transitions occur for either the Co^{3+} or the Co^{4+} ions for $0 \leq y \leq 0.67$. Thus, we assumed the IS state of Co^{4+} for the entire range of y and calculated p_{eff} for combinations with the LS, IS, and HS states of Co^{3+}. As shown in Fig. 9, the combination of IS-Co^{4+} and IS-Co^{3+} accounts very well for the observed values of p_{eff} up to $y=0.67$. The intermediate spin states for both Co^{4+} and Co^{3+} have also been reported for the 3D perovskite of $La_{0.5}Ba_{0.5}CoO_3$.[12]

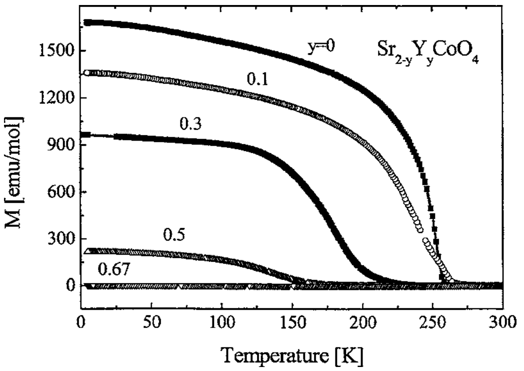

FIG. 6. Temperature dependence of the field cooled dc magnetization measured at a magnetic field of 20 Oe.

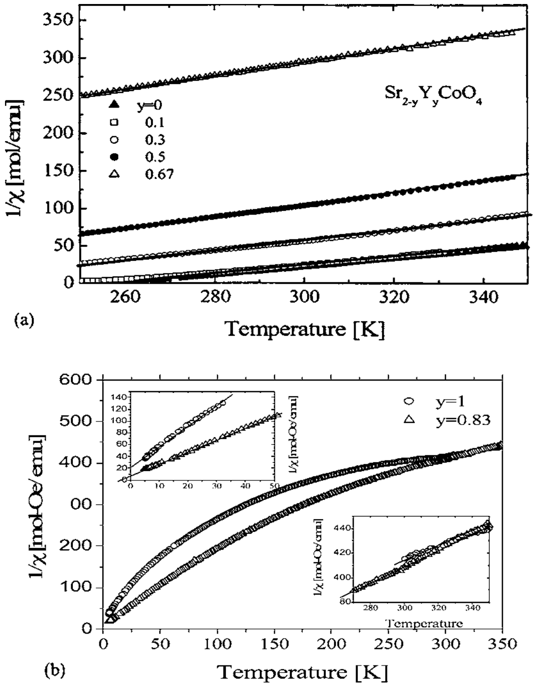

FIG. 7. Temperature dependence of the inverse molar susceptibility, χ^{-1}, measured at a magnetic field of 2 kOe for $y=0-0.67$ (a) and $y=0.83$ and 1.0 (b). Insets in (b) show linear fittings at high and low temperature ranges.

As shown in Fig. 7, the susceptibility data for $y=0.83$ or 1.0 do not obey the Curie-Weiss equation. Both sets of χ^{-1} data describe curved lines for the entire range of temperature without any ranges of linearity. An approximate linear fitting for the data in the higher temperature region gives $p_{eff}=3.51$ and 3.83, in $y=0.83$ and 1.0, respectively [see right inset of Fig. 7(b)]. On the other hand, fitting for the low-temperature data gives $p_{eff}=2.02$ and 1.50 in $y=0.83$ and 1.0, respectively [see a inset of Fig. 7(b)]. Although these p_{eff} values are the results of very rough estimation, it seems that p_{eff} increases continuously with increasing temperature from ~ 2.0 (~ 1.5) below around 30 K to ~ 3.5 (~ 3.8) at around 300 K in $y=0.83$ (1.0). It has been reported that for the $La_{2-x}Sr_xCoO_4$ system ($0.4 \leq x \leq 1.0$), the spin state transition from HS to IS occurs in Co^{3+} as x increases beyond $x \sim 0.7$. The high temperature p_{eff} values for $y=0.83$ and 1.0 suggest that the HS state is mixed with the IS state in Co^{3+} and that the HS state becomes more dominant with increasing temperature and increasing y. On the other hand, p_{eff} estimated from the low-temperature data suggests mixing of the LS state of Co^{3+} with a higher ratio for lower temperature. These results suggest complicated spin states of Co^{3+} ions for the $y=0.83$ and 1.0 phases where the LS, IS, and HS states seem to be mixed depending on temperature and y. Here it is worth recalling that in Figs. 3 and 4, tetrahedral distortion of the CoO_6 octahedron is less pronounced for the high y range. Since IS state Co^{3+} has the largest Jahn-Teller stabilization energy, mixing of the HS and LS states of Co^{3+} would work to diminish the Jahn-Teller distortion, consistent with the tendencies in Figs. 3 and 4.

The 3D perovskite of $La_{1-x}Sr_xCoO_3$ is a good reference system for the present one. Substitution of Sr for La in

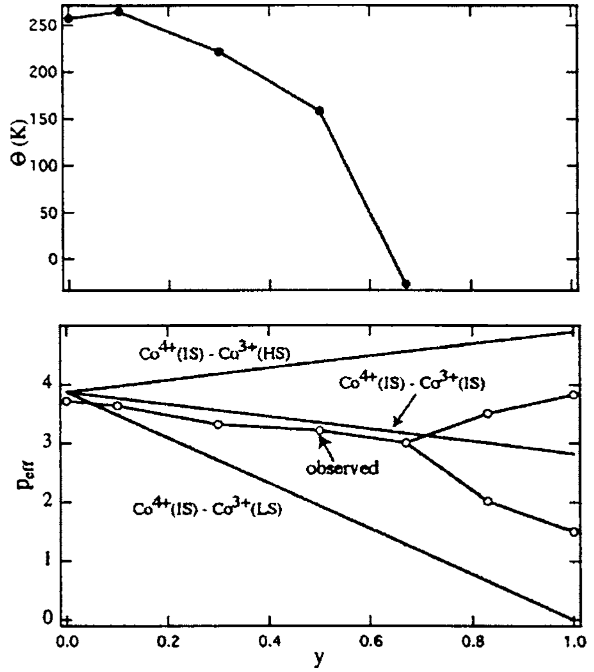

FIG. 8. The y dependences of Θ (upper panel) and p_{eff} (lower panel). Two p_{eff} values are given for $y=0.87$ (and $y=1$), in which the larger value was obtained from fitting the higher temperature susceptibility data while the smaller one comes from lower temperature data.

$LaCoO_3$ brings about remarkable changes; a semiconductor-to-metal transition is induced at $x=0.125-0.3$ and a nonmagnetic-to-ferromagnetic transition appears at $x=0.05-0.15$ with rather wide dispersion from report to report (see Ref. 8). Thus, the $x=0.5$ phase, $La_{0.5}Sr_{0.5}CoO_3$, is a good conductor with $\rho<10^{-4}\ \Omega$ cm and a ferromagnet with a saturation moment of $\sim 1.5\mu_B$/Co atom. Goodenough and his colleagues qualitatively explained the ferromagnetism of $La_{1-x}Sr_xCoO_3$ based on Zener's double exchange;[8,9] their model consists of localized t_{2g}^5 configurations ($S=1$) for each Co ion and an itinerant σ^* band which contains $1-x$ electrons per Co atom. Ferromagnetic coupling is expected between the itinerant and localized electrons, resulting in the ferromagnetic order of the localized electrons and polarization of the itinerant electrons. If we consider a pure ionic model for this situation, the system consists of the IS state of Co^{3+} and the HS state of Co^{4+} with a ferromagnetic coupling between them.

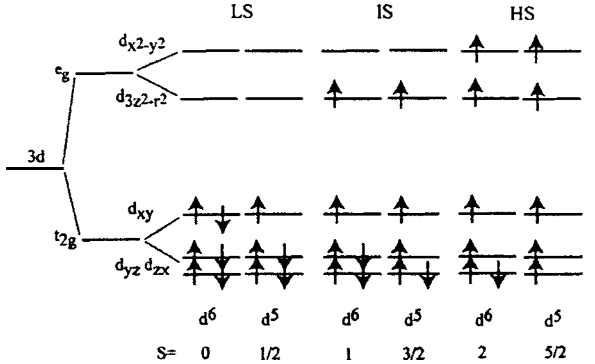

FIG. 9. Schematic representation of the electron energy levels for the Co^{3+} (d^6) and Co^{4+} (d^5) ions in a tetragonal crystal field.

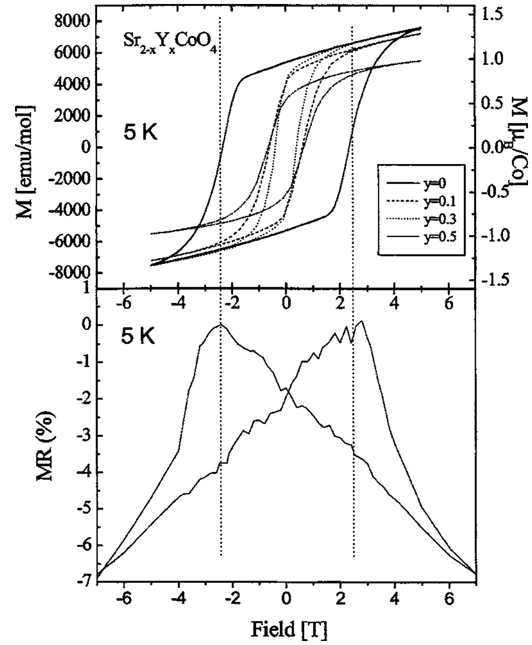

FIG. 10. Magnetic hysteresis loops for $Sr_{2-y}Y_yCoO_4$ and field-hysteretic magnetoresistance for Sr_2CoO_4 at 5 K.

Compared with the 3D system, e_g electrons of the present 2D system are expected to behave differently. In the 3D system, the σ^* band is formed from hybridization of Co-$3d_{z^2-r^2}$ and O-$2p$ orbitals along the c axis as well as from Co-$3d_{x^2-y^2}$ and O-$2p$ orbitals along the ab plane. In the layered structure, on the other hand, the σ^* band would be composed mainly of the $3d_{x^2-y^2}$ and O-$2p$ orbitals with a less significant contribution of the $3d_{z^2-r^2}$ orbitals due to the 2D confinement of the Co-O-Co network. Because of the tetragonal symmetry of the CoO_6 octahedron, both t_{2g} and e_g states are split into two levels as shown in Fig. 9. If electrons in orbitals other than $3d_{x^2-y^2}$ tend to be localized, we expect a semiconducting nature for the system with the IS (or LS) states of Co^{3+} and Co^{4+}. This picture may explain the lower electrical conductivity of the present system compared with the 3D perovskite system.

Magnetization and magnetic field loops at 5 K for $Sr_{2-y}Y_yCoO_4$ are shown in Fig. 10. The magnetization increases linearly with magnetic field in the high field range for all y values, i.e., the magnetization under high magnetic field can be expressed as $M=M_s+\chi_h H$ where M_s and χ_h stand for the saturation magnetization and the high field susceptibility, respectively. In Sr_2CoO_4, magnetization at 50 kOe is $\sim 1.5\mu_B$/Co atom and M_s at 5 K is estimated to be $\sim 1.0\mu_B$/Co atom, which is only 1/3 of the value of $3\mu_B$ expected for the saturation moment at 0 K for the IS state of Co^{4+} from the ionic model or 1/2.85 of the saturation moment corresponding to the observed p_{eff} of 3.72. As shown in Fig. 10, M_s decreases with increasing y to $0.75\mu_B$/Co atom for $y=0.5$. The Rhodes-Wohlfarth relationship is well known to be valid for itinerant ferromagnets with Curie-Weiss behavior above T_c. This relationship

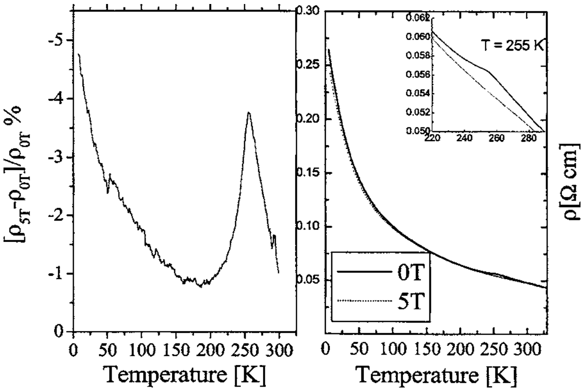

FIG. 11. The temperature dependences of the resistivity under 0 and 50 kOe (right panel) and magnetoresistance (left panel) for Sr_2CoO_4. Inset shows the resistivity within the temperature range around T_c.

was first given empirically,[24] then explained theoretically based on self-consistently renormalized (SCR) spin fluctuation theory.[25] The Rhodes-Wohlfarth ratio of p_c/p_s obeys a universal function of T_c where p_c and p_s, respectively, stand for the high temperature magnetic moment corresponding to p_{eff} and the saturation magnetic moment at 0 K in units of the Bohr magneton. From a Rhodes-Wohlfarth plot using the present ferromagnetic transition temperature of Sr_2CoO_4 (T_c=255 K), p_c/p_s was determined to be ~2.1. This value is comparable with ~3 or ~2.85 of the present experimental result. This result together with the linear increase of the magnetization in the high field range might suggest itinerant electron ferromagnetism for the present system.

Inconsistent with the itinerant electron picture, the magnetic susceptibility data of the higher temperature region can be well understood assuming localized electrons with the IS states of Co^{4+} and Co^{3+} for the phases with $y \leqslant 0.67$. Moriya *et al.* proposed, based on the SCR theory for itinerant electron magnets, that local spin fluctuation increases with temperature until it reaches an upper limit determined by the charge neutrality condition.[26,27] However, it is not clear that such a situation of temperature induced local magnetic moment is realized in the present system because its electrical resistivity is relatively high and shows semiconducting behavior even for $y \leqslant 0.5$. The ferromagnetism of the system may be explained on the basis of a localized electron picture. For instance, the saturation magnetization within the low temperature region, which is much smaller than that expected from p_{eff} in the higher temperature region may be caused by a certain temperature dependent combination of the HS and LS states. Thus, we need further studies to reach a conclusion on the origin of the ferromagnetism.

The very large coercive field of 25 kOe for Sr_2CoO_4 should be noted (Fig. 10); it implies a large anisotropy energy. The coercive field decreases with increasing y but is still large enough to be 2 kOe for y=0.5. In initial stages of the magnetization curve just after zero-field cooling to 5 K for Sr_2CoO_4 (see Fig. 10), magnetization increases stepwise as a function of magnetic field with a first steep increase, a plateau and then a second gradual increase. This phenomenon may also reflect the large anisotropy energy.

The temperature dependences of the resistivity for Sr_2CoO_4 under 0 and 50 kOe are compared in Fig. 11.There is a kink at 255 K in the zero field ρ-T curve of Sr_2CoO_4 as revealed in the inset of Fig. 11. This kink corresponds to the ferromagnetic transition at T_c of 255 K and is caused by a less pronounced increase of resistivity below T_c. In the field of 50 kOe, resistance decreases, and thekink seen at 255 K disappears completely. The magnetoresistance MR is defined as $\Delta\rho/\rho_0=(\rho_H\text{-}\rho_0)/\rho_0$ where ρ_0 and ρ_H stand for the resistivities under no magnetic field and magnetic field, respectively. The temperature variation of MR is shown in Fig. 11. It can be seen that $\Delta\rho/\rho_0$ is negative for the entire range of temperatures (negative magnetoresistance) and shows a sharp peak in the vicinity of the ferromagnetic transition at 255 K followed by a gradual increase with decreasing temperature. This behavior is quite similar to that observed in the 3D Co perovskite $La_{0.5}Ba_{0.5}CoO_3$.[12]

The peak in $\Delta\rho/\rho_0$ near the ferromagnetic transition temperature is explained by the intrinsic mechanism of magnetoresistance,[28] the ferromagnetic order is enhanced by the application of an external magnetic field, and it causes a decrease in the electrical resistivity. On the other hand, when the temperature decreases, field-hysteretic magnetoresistance corresponding to the magnetic hysteresis loop appears and becomes much more pronounced at 5 K as shown in Fig. 10. It can be seen that the maximum field-hysteretic $\Delta\rho/\rho_0$ occurs at a field of about 2.5 T, in coincidence with the coercive field of the magnetization process. Such a close correlation between the magnetoresistance and the magnetic domain rotation observed for our Sr_2CoO_4 sample can be well explained in terms of tunneling magnetoresistance at grain boundaries, a phenomenon that has been well established for granular manganites and other magnetresistive oxides.[28] Under the application of a magnetic field, the hopping of spin-polarized electrons between grains is predominantly affected by the relative angle between the magnetic moments of the grains and is controlled by the external field through the domain-rotation process. Therefore, the observed field-hysteretic magnetoresistance is ascribed to field suppression of the spin-dependent scattering at grain (or domain) boundaries.

IV. CONCLUSION

Layered perovskite cobalt oxides $Sr_{2-y}Y_yCoO_4$ (y=0, 0.1, 0.3, 0.5, 0.67, 0.83, and 1) were synthesized under high pressure and high temperature conditions. Structure refinement revealed that these compounds crystallize in K_2NiF_4-type structures with space group I4/mmm. The parent compound Sr_2CoO_4 undergoes a ferromagnetic transition with T_c =255 K. The T_c decreases with increasing y to 150 K for y =0.5, and ferromagnetism was not observed for $y>0.67$. Magnetic susceptibilities above T_c of the samples with $y \leqslant 0.67$ can be well fitted by the Curie-Weiss law and the effective number of Bohr magnetons, p_{eff}, determined from the Curie-Weiss constants, suggestingintermediate spin states for both the Co^{4+} and Co^{3+} ions. On the other hand, low temperature magnetization data suggest itinerant electron ferromagnetism. Fairly large negative magnetoresistance was observed for Sr_2CoO_4 near the ferromagnetic transition temperature of 255 K and in the lower temperature region. The magnetoresistance near T_c is explained by the intrinsic mechanism while that at lower temperatures is ascribed to the field suppression of the spin-dependent scattering at grain (or domain) boundaries.

ACKNOWLEDGMENTS

The authors would like to thank H. Sakurai, T. Nagai, and Y. Matsui of NIMS for fruitful discussions and T. Silver of ISEM for careful reading of this paper. This study was partially supported by Grants-in-Aid for Scientific Research from the Japan Society for the Promotion of Science (Grants Nos. 16076209, 16340111).

---

*Electronic address: muromachi.eiji@nims.go.jp

[1] M. A. Senarfs-Rodriguez and J. B. Goodenough, J. Solid State Chem. **116**, 224 (1995), and references therein.

[2] M. A. Korotin, S. Yu. Ezhov, I. V. Solovyev, V. I. Anisimov, D. I. Khomskii, and G. A. Sawatzky, Phys. Rev. B **54**, 5309 (1996).

[3] P. Ravindran, H. Fjellvåg, A. Kjekshus, P. Blaha, K. Schwarz, and J. Luitz, J. Appl. Phys. **91**, 291 (2002).

[4] T. Saitoh, T. Mizokawa, A. Fujimori, M. Abbate, Y. Takeda, and M. Takano, Phys. Rev. B **56**, 1290 (1997).

[5] S. Yamaguchi, Y. Okimoto, and Y. Tokura, Phys. Rev. B **55**, R8666 (1997).

[6] Y. Kobayashi, N. Fujiwara, S. Murata, K. Asai, and H. Yasuoka, Phys. Rev. B **62**, 410 (2000).

[7] C. Zobel, M. Kriener, D. Bruns, J. Baier, M. Grüninger, T. Lorenz, P. Reutler, and A. Revcolevschi, Phys. Rev. B **66**, 020402(R) (2002).

[8] M. A. Senarfs-Rodriguez and J. B. Goodenough, J. Solid State Chem. **118**, 323 (1995), and references therein.

[9] J. B. Goodenough, Mater. Res. Bull. **6**, 967 (1971).

[10] P. Ravindran, P. Korzhavyi, H. Fjellvag, and A. Kjekhus, Phys. Rev. B **60**, 16423 (1999).

[11] R. Potze, G. Sawatzky, and M. Abbate, Phys. Rev. B **51**, 11501 (1995).

[12] F. Fauth, E. Suard, and V. Caignaert, Phys. Rev. B **65**, 060401(R) (2002).

[13] T. Matsuura, J. Tabuchi, J. Mizusaki, Y. Yamauchi, and K. Fueki, J. Phys. Chem. Solids **49**, 1403 (1988), and references therein.

[14] T. Matsuura, J. Tabuchi, J. Mizusaki, Y. Yamauchi, and K. Fueki, J. Phys. Chem. Solids **49**, 1409 (1988).

[15] Y. Furulakawa, S. Wada, and Y. Yamada, J. Phys. Soc. Jpn. **62**, 1127 (1993).

[16] Y. Moritomo, K. Higashi, K. Matsuda, and A. Nakamura, Phys. Rev. B **55**, R14725 (1997).

[17] E. Iguchi, H. Nakatsugawa, and K. Futakuchi, J. Solid State Chem. **139**, 176 (1998).

[18] M. Itoh, M. Mori, Y. Moritomo, and A. Nakamura, Physica B **259**, 997 (1999).

[19] J. Wang, W. Zheng, and Y. Xing, Phys. Rev. B **62**, 14140 (2000).

[20] J. Wang, W. Zheng, and Y. Xing, J. Phys.: Condens. Matter **12**, 7425 (2000).

[21] B. A. Hunter, Commission Powder Diffraction Newsletter **20**, 21 (1998).

[22] Inorganic Crystal Structure Database, ICSD #20293; K. Lukaszewicz, Angew. Chem. **70**, 320 (1958).

[23] S. Ruddlesden and P. Popper, Acta Crystallogr. **10**, 538 (1957).

[24] P. Rhodes and E. P. Wohlfarth, Proc. R. Soc. London, Ser. A **273**, 247 (1963).

[25] Y. Takahashi, J. Phys. Soc. Jpn. **35**, 3553 (1986).

[26] T. Moriya, Solid State Commun. **26**, 483 (1978).

[27] Y. Takahashi and T. Moriya, J. Phys. Soc. Jpn. **46**, 1451 (1979).

[28] As a review, M. Ziese, Rep. Prog. Phys. **65**, 143 (2002).